

A CFD INVESTIGATION INTO MOLTEN METAL FLOW AND ITS SOLIDIFICATION UNDER GRAVITY SAND MOULDING IN PLUMBING COMPONENTS

Sirawit Namchanthra¹, Chakrit Suvanjumrat¹, Watcharapong Chookaew¹, Wichuphan Wijitdamkerng², and *Machimontorn Promtong¹

¹Department of Mechanical Engineering, Faculty of Engineering, Mahidol University, Salaya, Nakhon Pathom, 73170, Thailand

²Chaipong Engineering Ltd., Sam Phran, Nakhon Pathom 73210, Thailand

*Corresponding Author, Received: 30 Nov. 2021, Revised: 01 Feb. 2022, Accepted: 23 Feb. 2022

ABSTRACT: Metal casting using the solidification of molten metal flows involves complex heat transference during production. This can cause defects in the workpiece, affecting the efficiency of production. This research will use the Computational Fluid Dynamics (CFD) technique to investigate the filling, solidification, and cooling stages of the production of a component for plumbing. The CFD program FLOW 3D CAST v5.03 tracked the leading edge of the molten metal liquid (based on the Volume of Fluid (VOF) method). A two-equation $k-\epsilon$ turbulence was adopted to provide a Reynold term, and it should be noted that the geometry of the molten liquid and the internal chamber is the same as in the actual production line. The simulation shows how different pouring temperatures affect the runner, and that the pouring temperature influenced the behavior of the molten metal flow, resulting in defects on the workpiece. Moreover, the runner and its number affected the liquid metal flow and affected the defect's location during the solidification period. Future work will verify the results between the simulation and experiments, and further investigate possible defect locations on the surface of the workpiece, which could be a critical criterion in further discussions.

Keywords: Volume of Fluid (VOF) Method, Computational Fluid Dynamics (CFD), Gravity Sand Casting, Pouring Temperature, Solidification and Cooling Stages, Mould and Runner Design

1. INTRODUCTION

In the manufacturing of plumbing components, gravity sand casting is a commonly used production process. The casting process starts with the preparation of a sand mould, into which molten metal is poured. The metal solidifies during the cooling processes, after which the mould is removed, and the workpiece quality is checked for shape and size. If there are defects, the component cannot proceed to the finishing section and would be recycled to save the materials cost. Currently, many techniques have been proposed to enhance the economic efficiency of molten metal casting, such as the production of several castings in a single mould, as well as the introduction of lost foam technology [1]. This can increase the efficiency of material use and save production costs, but it requires a deep understanding of mould layout design, material pouring techniques, and the physical molten metal heat transfer process.

Defects in castings usually arise from poor design of the mould, and unsuitably sized runner, or carelessness during the pouring process [2, 3]. Fig. 1 shows plumbing components produced by casting as defective workpieces (Fig. 1c shows the defects (porosity) within the workpiece). The external and internal cavities affect the mechanical properties, resulting in low-quality casting that is unfit for

purpose. For decades, research has investigated the influence of pouring temperature, filling rate, pressure transfer (during the solidification period), cooling rates, mould coating material, and air entrapment behavior [1, 4-9] on the quality. Some works focused on minimizing residual stress and the healing of possible biofilms during solidification [10, 11]. Moreover, the magnetic fields were added to the solidification process to eliminate shrinkage defects [12]. Because of the parameter optimization (i.e., pouring temperature and pouring time), a mathematical model based on regression analysis was proposed recently [13].

The Computational Fluid Dynamics (CFD) technique is widely used in the casting process design, especially for parametric optimization [14-22]. This promising tool can help redesign the mould layout and eliminate defects such as shrinkage, porosity, and the discovery of hot spot regions [23], significantly, the liquid phase transformation to the solid phase, which could also capture using the CFD technique. This metallurgical process could point out critical criteria of defect occurrence [20].

Some researchers have observed the effects of the feeder and discussed concerns regarding the filling characteristics [23]. Moreover, the heat transfer and the interface between solids and liquids were identified as related to various casting speeds

[15]. Apart from the fluctuated surface of molten metal, the temperature distribution during the filling and solidification was intentionally monitored [18]. The validation study, and especially the casting process, became mandatory tasks so the evaluation was accurate [2, 6, 24-30].

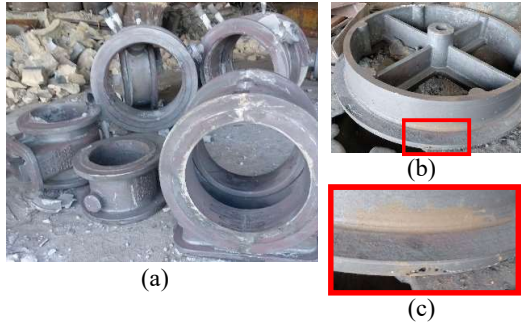


Fig. 1 Plumbing joints produced in the plumbing manufacturing process (Thailand); (a) examples of plumbing parts, (b) an example of defected part, and (c) a close-up view of the porosity occurrence

2. RESEARCH SIGNIFICANCE

To save the cost and time for parametric study, hence this research uses the Volume of Fluid (VOF) method to capture the molten metal flows in the gravity sand mould instead of doing experiments. The effects of different pouring temperatures and different internal structures on the traveling distance and filling time could be precisely observed. More importantly, the curve of average temperature during the solidification and cooling stages could also be observed. Overall, the objective of this work is to use the Computational Fluid Dynamics (CFD) technique:

- i) to investigate the molten metal flows during the filling stage, as well as the influence of pouring temperature,
- ii) to capture the casting process, especially the solidification when operating under different pouring temperatures,
- iii) to analyze the effects of the size and number of runners and discuss possible solutions to reduce the cavity defects.

It should be noted that a CFD program named FLOW CAST v5.03 was used to capture the filling, solidification, and cooling sequences. Therefore, the time for each stage will be included in additional discussions under the considered controlling conditions, from which insights may be observed. This will lead to suggestions for future improvements, especially reducing the cavity defects, decreasing the production time, and enhancing the product quality.

3. FLUID FLOW EQUATIONS AND VOLUME TRACKING METHOD

3.1 Fluid Flow Equations

To perform the casting simulation, FLOW 3D CAST will be used as it is a program that calculates based on the Fractional Area/Volume Obstacle Representation (FAVOR) method, which is based on the finite difference for the generated mesh. This technique may improve the accuracy of the numerical solution near the mould walls when compared to the standard finite-difference. For an incompressible, viscous fluid study, FAVOR equations are formulated using the flowing equations:

$$\nabla \cdot (\mathbf{A}\mathbf{u}) = 0 \quad (1)$$

$$\frac{\partial \mathbf{u}}{\partial t} + \frac{1}{V} (\mathbf{A}\mathbf{u} \cdot \nabla) \mathbf{u} = -\frac{1}{\rho} \nabla p + \frac{1}{\rho V} (\nabla \mathbf{A}) \cdot (\mu \nabla) \mathbf{u} + \mathbf{g} \quad (2)$$

$$\frac{\partial H}{\partial t} + \frac{1}{V} (\mathbf{A}\mathbf{u} \cdot \nabla) H = \frac{1}{\rho V} (\nabla \mathbf{A}) \cdot (k \nabla T) \quad (3)$$

$$\text{Where } \mathbf{A}\mathbf{u} = (A_x u_x, A_y u_y, A_z u_z)$$

$$(\nabla \mathbf{A}) = \left(\frac{\partial}{\partial x} A_x, \frac{\partial}{\partial y} A_y, \frac{\partial}{\partial z} A_z \right)$$

$$\mathbf{H} = \int C(T) dT + L(1 - f_s) \quad (4)$$

Where A_i is the open area fraction associated with the flow in the i^{th} direction. V , ρ , and p are the open volume fraction, density, pressure. Where u_i is the velocity component and μ is the fluid viscosity coefficient. g gravity, H fluid enthalpy, T fluid temperature, f_s solid fraction, L latent heat. C and k are the fluid-specific heat and thermal conductivity coefficients, respectively.

With regard to the temperature focus, the energy equation and its form are as follows:

$$\frac{\partial T_m}{\partial t} = \frac{1}{\rho c_m V_c} (\nabla A_c) \cdot (k_m \nabla T_m) \quad (5)$$

where m indicates the parameter related to the mould and c indicates quantities that are complements of the volume and area fractions. At the metal/mould interface, the heat flux, q , is calculated by

$$\mathbf{q} = h(\mathbf{T} - T_m) \quad (6)$$

where h is the heat transfer coefficient.

3.2 Volume of Fluid (VOF) Method

In the mould filling process, the boundaries between the molten casting metal and the surrounding air can be tracked using the tracking-free surface technique. In terms of numerical development, the most popular method to describe the free surfaces and deformations are the Volume-of-Fluid (VOF)

method. The equation for the VOF method is represented as the F function, which is shown as follows:

$$\frac{\partial F}{\partial t} + \frac{1}{v} \nabla \cdot (AuF) = 0 \quad (7)$$

The boundary conditions on the free surface have no normal and tangential stresses so the time step must assess the accuracy and stability. As in Eq. 8, the accuracy of the results is constant when the time step is less than the minimum value of the calculated ratio. The time increment for stability is necessarily governed by two restrictions, firstly the fluid material cannot move through more than one cell in the one-time step because the different equations assume fluxes between adjacent cells only. Therefore, the time increment must satisfy the inequality below.

$$\Delta t < \min \left\{ \frac{\Delta x_i}{|u_{i,j}|}, \frac{\Delta y_j}{|v_{i,j}|} \right\} \quad (8)$$

where the mesh increments, Δ and $\Delta \mathbf{x}$, u and v , velocity component, and the time increment, Δt . The minimum is calculated concerning every cell in the mesh. Typically, Δt is equal to one-fourth to one-third of the minimum cell transit time. Secondly, where there is a non-zero value for kinematic viscosity, momentum must not be diffused by more than approximately one cell in a one-time step. A linear stability analysis shows that this limitation by

$$v\Delta t < \frac{1}{2} \frac{\Delta x_i^2 \Delta y_j^2}{\Delta x_i^2 + \Delta y_j^2} \quad (9)$$

with Δt satisfying the two inequalities above. The last parameter that ensures numerical stability is α , the upstream differencing parameter. The proper choice for α is

$$1 \geq \alpha > \max \left\{ \left| \frac{u_{i,j}\Delta t}{\Delta x_i} \right|, \left| \frac{v_{i,j}\Delta t}{\Delta y_i} \right| \right\} \quad (10)$$

Further information regarding the VOF method can be found in the research papers of Hirt [31] and Aniszewski [32].

4. DETAILS OF THE NUMERICAL STUDY

The plumbing component is used to simulate the study and it was created in the stereolithography (STL) format and imported into the FLOW 3D CAST software. Details of the model's multi-block meshes are shown in Fig. 3, and the thermophysical properties of the cast iron and sand mould are shown in Table 1. The surface roughness of the mould was $25 \mu\text{m}$, and the contact angle was 180° . The volume flow rate at the sprue was $0.0016 \text{ m}^3/\text{s}$, which was

calculated using the total weight of the molten metal and the filling time.

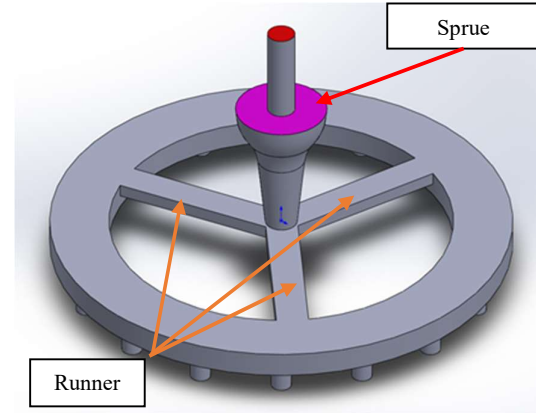


Fig. 2 A 3d model of the plumbing component where the red area is the cast iron inlet, and the pink area is the environment boundary.

5. RESULTS AND DISCUSSIONS

5.1 Mesh Independence Study

To minimize the calculation time, a mesh independence study was performed. In this study, the average temperature after the filling stage was derived from a comparison of different meshes. Fig. 3 shows how the multi-blocks are applied for the mesh of the plumbing component. The mesh was the smallest available size in the plumbing block (denoted by the blue box).

Four different meshes (3,600,000, 1,500,000, 250,000 and 20,000 elements) were tested and their average molten cast iron temperature compared (shown in Table 2).

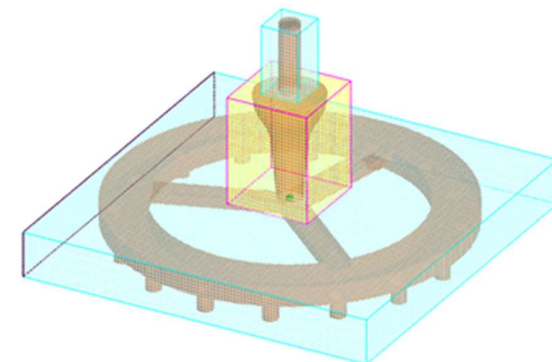


Fig. 3 The multi-block meshes of the plumbing component (the mould mesh is not displayed).

Table 1 Thermo-physical properties of the casting & mould used in the simulations

Material	Property	Symbol	Value	Unit
Casting	Thermal conductivity of the liquid	k_l	39.59	W/(mK)
	Thermal conductivity of the solid	k_s	34.39	W/(mK)
	Specific heat of the liquid	C_l	897	J/(kg K)
	Specific heat of the solid	C_s	770	J/(kg K)
	Surface tension coefficient of the liquid	σ	1.871	kg/s ²
	Kinematic viscosity	μ	0.004516* 0.0045* 0.00448539*	m ² /s
	The density of the liquid	ρ_l	6856	kg/m ³
	The density of the solid	ρ_s	7100	kg/m ³
	Latent heat	L	216	kJ/m ³
	Liquidus temperature	T_l	1230.5	deg-C
	Solidus temperature	T_s	1146.5	deg-C
Sand mould	Thermal conductivity	k_m	0.61	W/(mK)
	Volumetric specific heat	ρC	1700	kJ/(kg K)

Note: Three viscosities are for molten cast iron at 1329, 1429, and 1529 deg-C respectively.

The pouring temperature was 1429 deg-C (which is relevant to the real operation), and after the liquid was poured, the average temperature was reduced to a certain value due to the heat transfer to the mould. As shown in Table 1, the average temperatures created by the three different meshes are different, with a maximum of approximately 0.5%. Therefore, the smallest mesh size (250,000) was introduced for further study as the plumbing part component is small so the average temperature will not have much variance.

Table 2 The percentage difference of the average temperature at the end of the filling stage of different mesh sizes

Mesh	The average temperature on finish time (deg-C)	Error (%)
250,000	1401.49	0.447
1,500,000	1395.22	0.037
3,600,000	1394.70	-

5.2 Simulation of Plumbing Part

The filling of the molten liquid in the mould at different time are shown in Fig. 4. The cast iron melt at 1429 deg-C enters the mould at the pouring cup and keeps filling up the plumbing part. Fig. 4a shows the

filling at 1s, currently only a small volume of the liquid gets into the plumbing region. Fig. 4b and 4c show the melt entering the mould cavity and then completed filling the cavity about 9s. Afterward, the liquid keeps running back to the runner and fills the mould and ending at 10.861s (see (Fig. 4d)). It should be noted that in this simulation the fill fraction criteria for stopping the calculation was set at 0.999. At the finishing time of the filling process, the lowest temperature in the mould was lower than the pouring temperature about 35 deg-C.

Fig. 5. shows the solidification stage of the plumbing part, after the filling period. This process is very important because having the entrapped air in the mould could lead to the defect occurrence. From the figure, the melt solidification is started from the bottom part to the runner and the pouring area. As shown in Fig. 5a., reaching 0.6 solid fractions, it takes about 324s. The solidification reaches 0.9 of the solid fractions when the time is 529s, at this time, just only the basin region is not completely solidified (see Fig. 5b). Fig. 5c shows the time consumed and the solidified volume fraction. According to the graph, the solidified process slowly increases from 0 to 0.05 at the beginning (0-100s) and rapidly increased from 0.05 to 0.9 (100s-500s). After that, there has a slight increase until getting 0.999 of the solid fractions (~840s or ~ 14 mins).

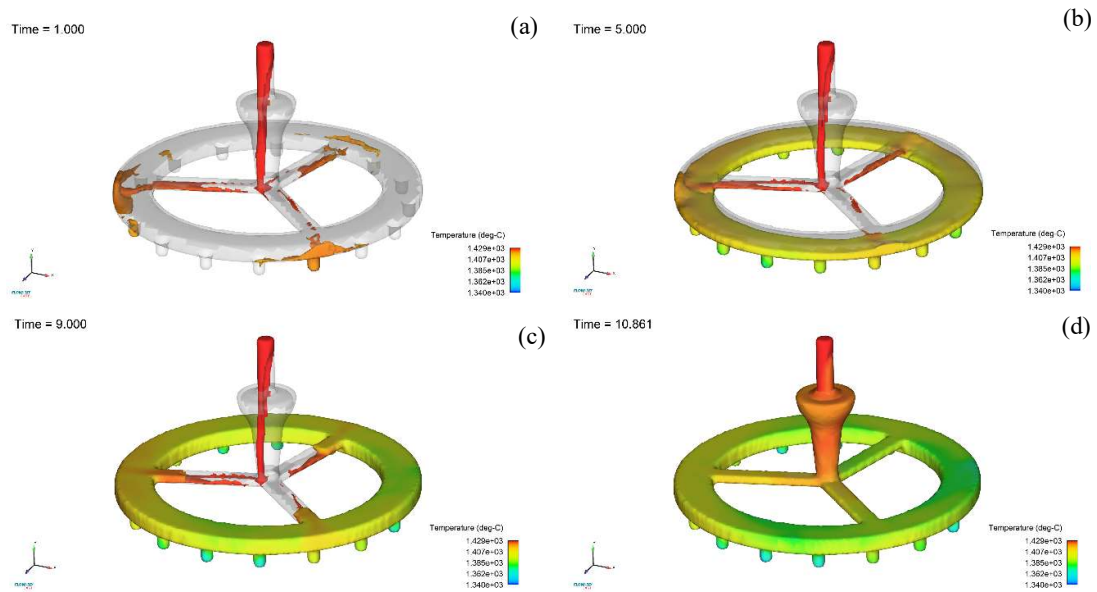


Fig. 4 The filling for the plumbing component at different times: (a) 1sec, (b) 5sec, (c) 9sec, and (d) 10.861sec.

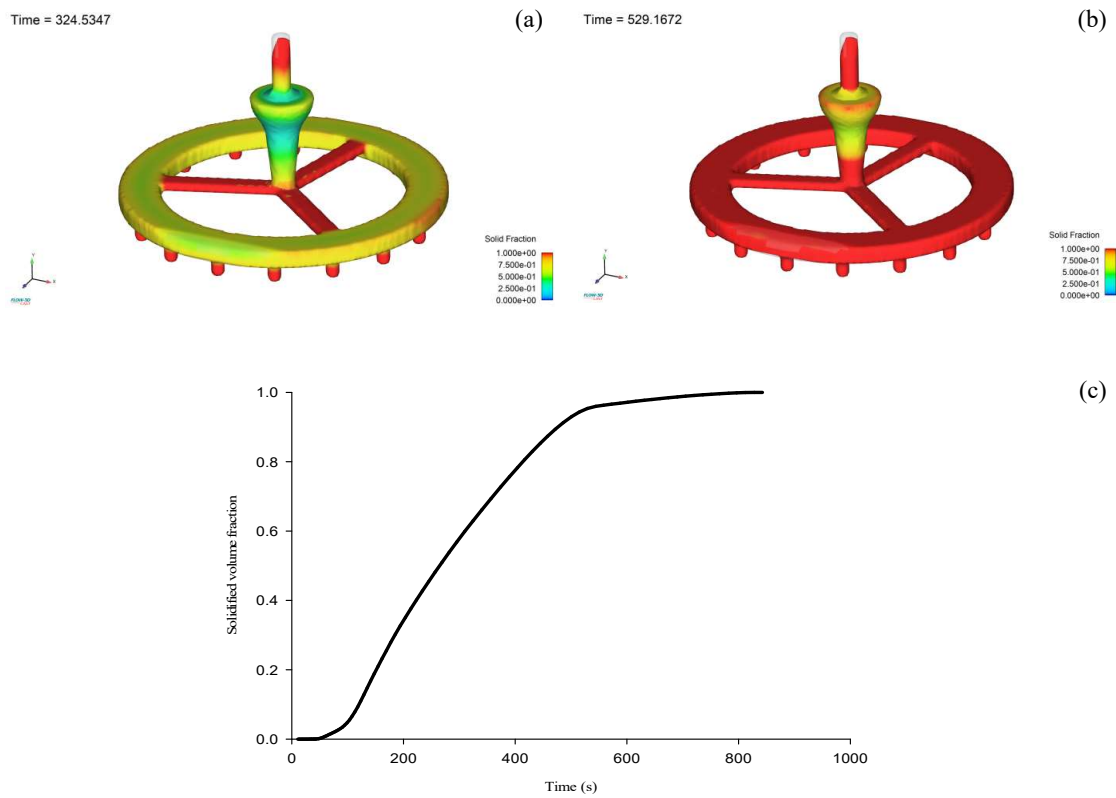


Fig. 5 The solidification of the plumbing component at (a) 0.6 solid fraction, (b) 0.9 solid fraction, and (c) solidified volume fraction through the solidification process

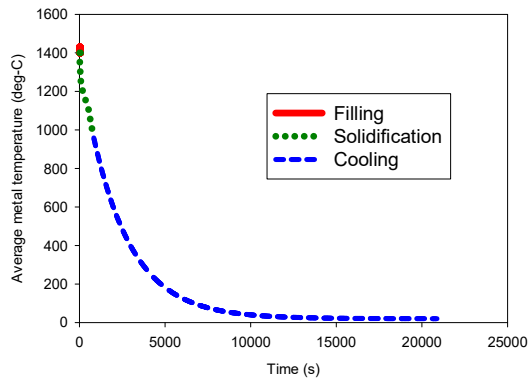


Fig. 6 Average temperature occurrence during the filling, solidification, & cooling stages (pouring temperature = 1429 deg-C)

Fig. 6 illustrates the average temperature and time consumed for the filling, solidification, and cooling stages. According to simulation results, the filling required 11 seconds, and the average temperature was reduced from 1429 °C to be approximately 1395 °C. During the solidification stage, 14 minutes (840 secs) were required. The solidification process was halted when the whole domain had 0.999 of the solid fractions when the average temperature was found at 962 °C. The cooling stage was longer than the other stages at more than five and a half hours before it reached ambient temperature.

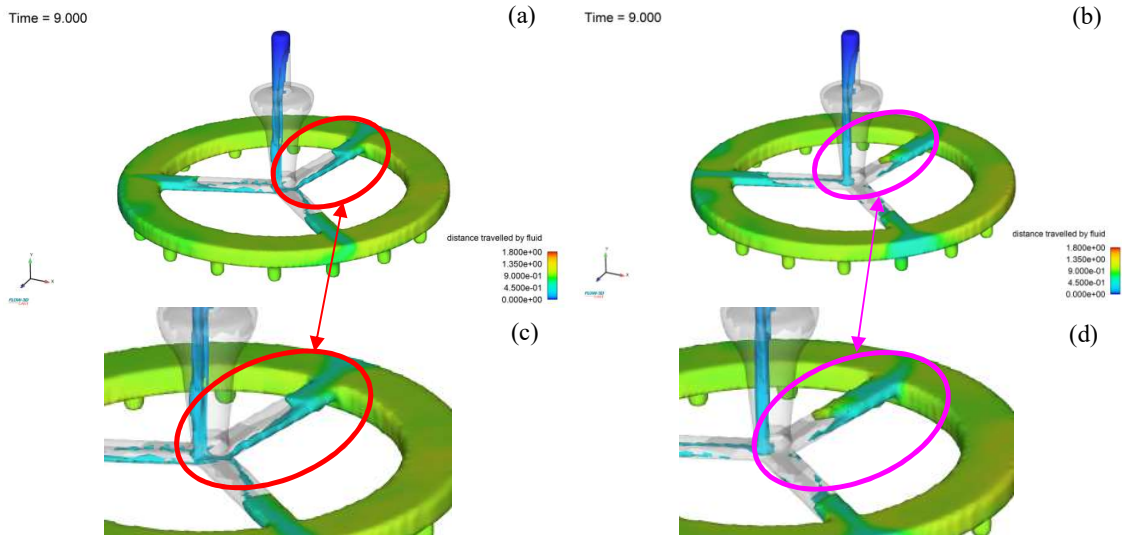


Fig. 7 Contour of distance travelled by the molten metal on 9s at (a) 1329 deg-C, (b) 1529 deg-C of the pouring temperature, (c) a close-up view of 1329 deg-C, and (d) a close-up view of 1529 deg-C

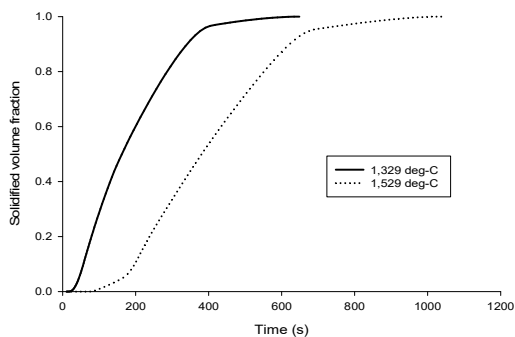


Fig. 8 Comparison of the solidified volume fraction of each pouring temperature through the solidification process

5.3 The Influence of The Pouring Temperature

Due to a requirement to study the influence of the pouring temperature, thus, in this simulation, two different cases having the temperature at 1329 deg-C and 1529 deg-C were investigated. Fig.7 shows the distance travelled by the fluid at the pouring time at 9 s. From the figures, it can be noticed the position of melted cast iron at 1529 deg-C flows faster than 1329 deg-C as confirmed by Fig. 7c and 7d. This could be because the higher pouring temperature has a lower viscosity, hence the melt can flow faster.

In this study, the solidification of melt cast iron on 1329 deg-C and 1529 deg-C were also compared and discussed the time-consuming.

Table 3 The solidification of the plumbing component at 0.6 and 0.9 solid fraction comparing between the cases 1329 deg-C and 1529 deg-C of pouring temperatures.

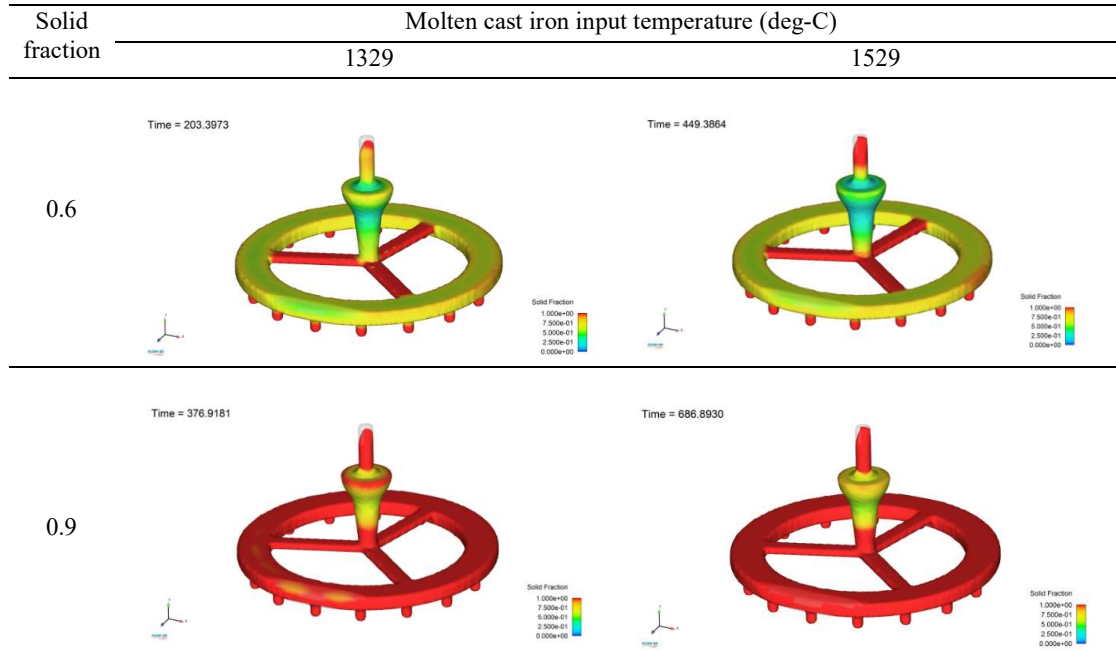


Table 3 shows the results at 0.6 and 0.9 of the solid fractions for the different pouring temperatures. The time consumed for each case to reach 0.6 of the solid fractions is approximately 200 seconds and 450 seconds respectively. For the case of reaching 0.9 of the solid fractions, the time required for the different pouring temperatures is approximately 376 seconds and 687 seconds at 1329 deg-C respectively. In general, the first solidified volume was found at the

lowest point of the plumbing component, at the runner, and at the last area to solidify, as shown in Table 3. The solidification graph (Fig. 8) shows that the solidification of the two different pouring temperatures was similar. at the beginning of the period, but the higher temperature case had slower growth compared to the case of having lower pouring temperature. This can affect the quality of the final workpieces, but further study is required to confirm this prediction.

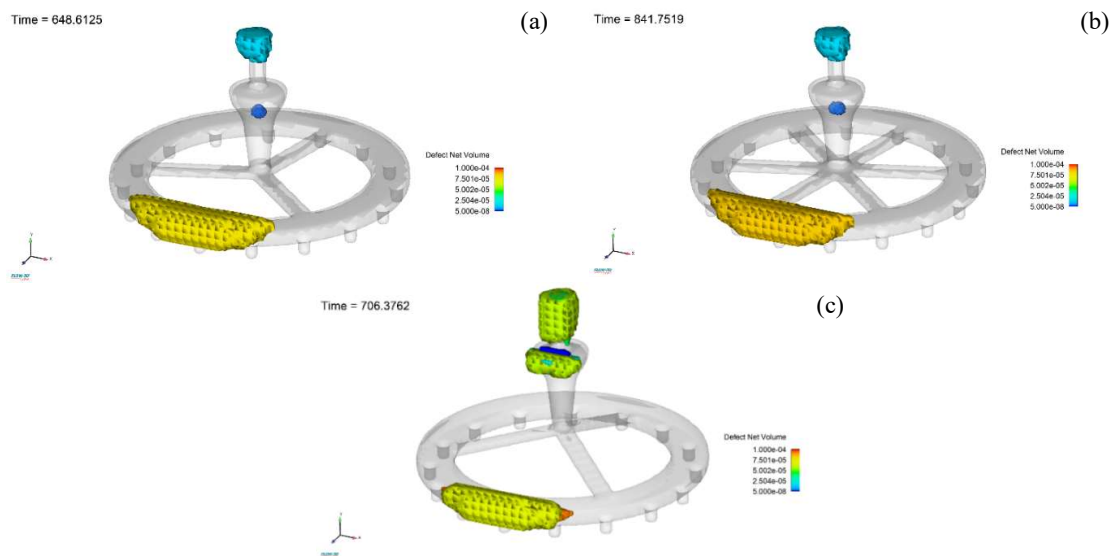


Fig. 9 Defect net volume on 1329 deg-C of the case (a) 3 branches runners, (b) 6 branches runners, and (c) 3 branches 15-degree inclined runners

5.4 Influence of The Runner Structure

The cavity found in the plumbing component was removed. Other possible defects occurred, and modifications to the runner were attempted. Three different angles were investigated, and the pouring temperature of the molten cast iron was 1329 deg-C. More details of the modified runners can be seen in Fig.9.

After the solidification was completed, the defect net volume (the volume of void) in the mould and its position were identifiable. It was found the defect location was the same in all cases, and the defect net volume was also similar, at approximately 1.0×10^{-4} (see Fig. 9). Therefore, the new modifications to the runner did not reduce the cavity defects in the plumbing component, possibly because of having no riser. Further investigation regarding the runner modifications study will be conducted in future work.

6. CONCLUSIONS AND FUTURE WORKS

The simulation of casting molten iron in the plumbing component was successfully performed using the CFD technique. The parameters affecting the quality of casting related to the cavity defect were investigated. Overall, the conclusions can be drawn as follows:

i) At the temperature of 1429 deg-C, the filling time required is 11 seconds, the solidification stage required 14 minutes, and the cooling time was around five and half hours.

ii) At different pouring temperatures (1329 and 1529 deg-C), the distance was traveled faster by molten cast iron with a higher temperature as it was less viscous. When comparing the solidification behavior, the time required to become solid for the case having a higher pouring temperature (1529 deg-C) was required nearly double the lower temperature.

iii) Introducing three different types of runners has no effect in terms of reducing the number of defects at the present work.

In future work, the experiment of pouring temperature will be conducted, and the data will be compared with simulation results. The parameters affecting the reasons behind the cavity defect will be discussed and a lower cost of production sought.

7. ACKNOWLEDGMENTS

This research was supported by the Mechanical Engineering Department, Faculty of Engineering, Mahidol University. Thanks to CADFEM SEA Pte. Ltd. - A Certified Elite Channel Partner to ANSYS - for providing support and access to the CFD program named ANSYS Fluent 2021 R1.

Also, the authors would like to thank Chaipong Engineering Co., Ltd. for allowing to use the facilities, and special thanks to Robert McEvoy, from

the Faculty of ICT at Mahidol University for editing and proofreading the manuscript.

8. REFERENCES

- [1] Deev V.B., Ponomareva K.V., Prikhodko O.G., and Smetanyuk S.V., Influence of temperatures of melt overheating and pouring on the quality of aluminum alloy lost foam castings. *Russian Journal of Non-Ferrous Metals*, 2017. 58(4): p. 373-377.
- [2] Ayar M.S., Ayar V.S., and George P.M., Simulation and experimental validation for defect reduction in geometry varied aluminum plates cast using sand casting. *Materials Today: Proceedings*, 2020. 27: p. 1422-1430.
- [3] Borikar G.P., and Chavan S.T., Optimization of Casting Yield in Multi-cavity Sand Moulds of Al-alloy Components. *Materials Today: Proceedings*, 2020. 28: p. 819-824.
- [4] Zhao H.-D., Bai Y.-F., Ouyang X.-X., and Dong P.-Y., Simulation of mold filling and prediction of gas entrapment on practical high pressure die castings. *Transactions of Nonferrous Metals Society of China*, 2010. 20(11): p. 2064-2070.
- [5] Li Y., Liu J., Zhong G., Huang W., and Zou R., Analysis of a diesel engine cylinder head failure caused by casting porosity defects. *Engineering Failure Analysis*, 2021. 127.
- [6] Dou K., Lordan E., Zhang Y., Jacot A., and Fan Z., A novel approach to optimize mechanical properties for aluminum alloy in High pressure die casting (HPDC) process combining experiment and modeling. *Journal of Materials Processing Technology*, 2021. 296.
- [7] Pulisheru K.S. and Birru A.K., Effect of pouring temperature on hot tearing susceptibility of Al-Cu cast Alloy: Casting simulation. *Materials Today: Proceedings*, 2021.
- [8] Pulivarti S.R. and Birru A.K., Effect of Mould Coatings and Pouring Temperature on the Fluidity of Different Thin Cross-Sections of A206 Alloy by Sand Casting. *Transactions of the Indian Institute of Metals*, 2018. 71(7): p. 1735-1745.
- [9] Li Y., Liu J., Zhang Q., and Huang W., Casting defects and microstructure distribution characteristics of the aluminum alloy cylinder head with complex structure. *Materials Today Communications*, 2021. 27.
- [10] Sarkar C., Gawande S.H., and Keste A.A., Design optimization of precision casting for residual stress reduction. *Journal of Computational Design and Engineering*, 2016. 3(2): p. 140-150.
- [11] Gopalan R. and Prabhu N.K., Oxide bifilms in aluminum alloy castings – a review. *Materials Science and Technology*, 2013. 27(12): p. 1757-1769.

- [12] Luo L., Xia H.-Y., Luo L.-S., Su Y.-Q., Cai C.-J., Wang L., Guo J.-J., and Fu H.-Z., Eliminating shrinkage defects and improving the mechanical performance of large thin-walled ZL205A alloy castings by coupling traveling magnetic fields with sequential solidification. *Transactions of Nonferrous Metals Society of China*, 2021. 31(4): p. 865-877.
- [13] Nandagopal M., Sivakumar K., and Sengottuvelan M., Process parameter optimization to reduce cold metal defect in ferrous casting using Taguchi technique and regression analysis. *Materials Today: Proceedings*, 2021. 45: p. 7917-7921.
- [14] Yang W., Luo Z., Zou Z., Zhao C., and You Y., Modelling and analysis of bubble entrapment by solidification shell in steel continuous casting considering bubble interaction with a coupled CFD-DBM approach. *Powder Technology*, 2021. 390: p. 387-400.
- [15] Loon W.L., Reddy S.S., and A.K. R.P., CFD simulation of direct chill casting process of magnesium alloy billets. *Journal of Manufacturing Processes*, 2019. 45: p. 447-454.
- [16] YIN J., Numerical modeling of the centrifugal casting process. 2016, KTH ROYAL INSTITUTE OF TECHNOLOGY.
- [17] Reicher A., Numerical Analysis of Die-Casting Process in Thin Cavities Using Lubrication Approximation. 2012, University of Wisconsin-Milwaukee.
- [18] Yuwen X.-X., Chen L., and Han Y.-J., Numerical Simulation of Casting Filling Process Based on FLUENT. *Energy Procedia*, 2012. 17: p. 1864-1871.
- [19] Kermanpur A., Mahmoudi S., and Hajipour A., Numerical simulation of metal flow and solidification in the multi-cavity casting molds of automotive components. *Journal of Materials Processing Technology*, 2008. 206(1-3): p. 62-68.
- [20] Vijayaram T.R., Sulaiman S., Hamouda A.M.S., and Ahmad M.H.M., Numerical simulation of casting solidification in permanent metallic molds. *Journal of Materials Processing Technology*, 2006. 178(1-3): p. 29-33.
- [21] Reikher A. and Pillai K.M., A fast simulation of transient metal flow and solidification in a narrow channel. Part I: Model development using lubrication approximation. *International Journal of Heat and Mass Transfer*, 2013. 60: p. 797-805.
- [22] Reikher A. and Pillai K.M., A fast simulation of transient metal flow and solidification in a narrow channel. Part II. Model validation and parametric study. *International Journal of Heat and Mass Transfer*, 2013. 60: p. 806-815.
- [23] Wang H., Djambazov G., Pericleous K.A., Harding R.A., and Wickins M., Modelling the dynamics of the tilt-casting process and the effect of the mould design on the casting quality. *Computers & Fluids*, 2011. 42(1): p. 92-101.
- [24] Aravind S., Ragupathi P., and Vignesh G., Numerical and experimental approach to eliminate defects in Al alloy pump- crankcase processed through gravity die casting route. *Materials Today: Proceedings*, 2021. 37: p. 1772-1777.
- [25] Barot R.P. and Ayar V.S., Casting simulation and defect identification of geometry varied plates with experimental validation. *Materials Today: Proceedings*, 2020. 26: p. 2754-2762.
- [26] Promptong M., Kasemjirapatara C., Srithep P., Masoodi Y., Namchanthra S., Priyadumkol J., and Suvanjumrat C., Investigation of Aerodynamic Performance of Four Potential Airfoils for a Formula SAE Car: A 2D Validation Study, in *The 34th Conference of the Mechanical Engineering Network of Thailand*. 2020: 15 - 17 July 2020, Prachuap Khiri Khan, Thailand.
- [27] Promptong M., Khunsri K., Teachapanitvittaya K., Trakulkumrue T., Watechagit S., and Suvanjumrat C., Experimental and Numerical Investigations into the Natural Convection of Hot Gas in a Vertical Smoking Oven: A Validation Study, in *The 34th Conference of the Mechanical Engineering Network of Thailand*. 2020: 15 - 17 July 2020, Prachuap Khiri Khan, Thailand.
- [28] Promptong M., Cheung S., Yeoh G., Vahaji S., and Tu J., CFD investigation of sub-cooled boiling flow using a mechanistic wall heat partitioning approach with Wet-Steam properties. *The Journal of Computational Multiphase Flows*, 2018. 10(4): p. 239-258.
- [29] Promptong M., Cheung S., and Tu J., Numerical modelling of subcooled boiling flow based on mechanistic approach: A validation study using wet steam (IAPWS) as working fluid properties. *Lecture notes in engineering and computer science*, 2016.
- [30] Promptong M. and Tekasakul P., CFD study of flow in natural rubber smoking-room: I. Validation with the present smoking room. *Applied Thermal Engineering*, 2007. 27(11-12): p. 2113-2121.
- [31] Hirt C.W. and Nichols B.D., Volume of Fluid (VOF) method for the dynamics of free boundaries. *Journal of Computational Physics*, 1981. 39(1): p. 201-225.
- [32] Aniszewski W., Ménard T., and Marek M., Volume of Fluid (VOF) type advection methods in two-phase flow: A comparative study. *Computers & Fluids*, 2014. 97: p. 52-73.